Ultraviolet camera measurements of passive and explosive (strombolian) sulphur dioxide emissions at Yasur volcano, Vanuatu

Ilanko, T.[1], Pering, T.D.[1*] Wilkes, T.C[1]., Woitischek, J.[2,3], D'Aleo, R.[4], Aiuppa, A[5]., McGonigle, A.J.S[1,6,7]., Edmonds, M[2]., Garaebiti, E.[8]

[1] Department of Geography, University of Sheffield, Winter Street, Sheffield, S10 2TN, UK
[2] Department of Earth Sciences, University of Cambridge, Downing Street, Cambridge, CB2 3EQ, UK
[3] BPI Institute, BP Institute, University of Cambridge, Madingley Rd, CB3 E0EZ, UK
[4] INGV, Sezione di Palermo, Via Ugo la Malfa 153, 90146, Palermo, Italy
[5] DiSTeM, Università di Palermo, Via Archirafi, 22, 90123 Palermo, Italy
[6] School of Geosciences, the University of Sydney, NSW2006, Australia
[7] Faculty of Health, Engineering and Sciences, University of Southern Queensland, Toowoomba, QLD 4350, Australia
[8] Geohazards Division, Vanuatu Meteorology and Geo-hazards Department, Lini Highway, Port Vila, Vanuatu

*Corresponding author: t.pering@sheffield.ac.uk

Abstract

Here, we present the first ultraviolet (UV) camera measurements of sulphur dioxide (SO_2) flux from Yasur volcano, Vanuatu, for the period 6th – 9th July 2018. These data yield the first direct gas measurement-derived calculations of explosion gas masses at Yasur. Yasur typically exhibits persistent passive gas release interspersed with frequent strombolian explosions. We used compact forms of the 'PiCam' Raspberry Pi UV Camera system (Wilkes et al., 2017, 2016) powered through solar panels to collect images. Our daily median SO_2 fluxes range from 4.0 – 5.1 kg s^{-1}, with a measurement uncertainty of -12.2% to +14.7%, including errors from: gas cell calibration drift, uncertainties in plume direction and distance, as well as plume velocity. This work highlights the use of particle image velocimetry (PIV) for plume velocity determination, which was preferred over the typically used cross-correlation and optical flow methods because of the ability to function over a variety of plume conditions. We calculate SO_2 masses for strombolian explosions of 8 – 81 kg (mean of 32 kg), which is, to our knowledge, the first budget of explosive gas masses from this target. Through the use of a simple statistical measure using the moving minimum, we estimate that passive degassing is the dominant mode of gas emission at Yasur, supplying an average of ~69% of the total gas released. Our work further highlights the utility of UV camera measurements in volcanology and, in particular, the benefit of the multiple camera approach in error characterisation. This work also adds to our inventory of gas-based data to characterise the spectrum of strombolian activity across the globe.

Highlights

- Long time series data collected using portable solar chargeable UV cameras.
- Particle image velocimetry (PIV) used for plume velocity measurements.
- Daily median SO_2 fluxes of 4.0-5.1 kg s^{-1}.
- SO_2 masses produced by strombolian explosions range 8 to 81 kg (mean 32 kg).

1. Introduction

Strombolian volcanism is one of the more common forms of basaltic explosive activity globally, associated with the rapid ejection of hot pyroclasts from a vent in a single impulsive burst (Blackburn et al., 1976; Taddeucci et al., 2015), with event frequencies ranging from seconds to minutes (Pering and McGonigle, 2018). Volcanoes with frequent strombolian activity include: the archetypal Stromboli, Italy (Patrick et al., 2007; Ripepe et al., 2002); Pacaya, Guatemala (Battaglia et al., 2018; Dalton et al., 2010); Erebus, Antarctica (Ilanko et al., 2015; Johnson and Aster, 2005; Oppenheimer et al., 2009; Sweeney et al., 2008); and Yasur, Vanuatu (Bani and Lardy, 2007; Kremers et al., 2013; Oppenheimer et al., 2006), the subject of this study. Other volcanoes also known to produce strombolian activity include: Etna, Italy (Aiuppa et al., 2016; Branca and Del Carlo, 2005; Pering et al., 2015) Villarrica, Chile (Shinohara and Witter, 2005); Arenal, Costa Rica (Garcés et al., 1998; Szramek et al., 2006); Batu Tara, Indonesia (Gaudin et al., 2017a; Laiolo et al., 2018); and Shishaldin, USA (Vergniolle et al., 2004).

Classically, this style of behaviour has been related to the ascent from depth of elongated and over-pressured bubbles, termed gas slugs (Taylor bubbles), which rapidly expand in length as they approach the surface, (Del Bello et al., 2012; James et al., 2008; Seyfried and Freundt, 2000; Taddeucci et al., 2015). However, recent research has suggested that the causal mechanisms may be far more diverse (Barth et al., 2019; Suckale et al., 2016; Woitischek et al., 2020), and that the presence of crystal-rich layers in the magmatic column is important in the mechanism of strombolian explosions. To test these hypotheses, it is useful to investigate the spectrum of strombolian activity at volcanoes, including Yasur, where this behaviour is typical. In addition, recent studies have highlighted the importance of eruption frequency in determining the behaviour of ascending gas slugs (Gaudin et al., 2017a) as well as inter-slug interactions (Pering et al., 2017, 2015). This has led to a classification of behaviour styles ranging from rapidly bursting slugs which may interact with one another during ascent, through to single bursting slugs (Pering et al., 2017; Pering and McGonigle, 2018).

There are several methods to obtain information about individual strombolian explosions, based on capture of: seismic (Chouet et al., 2003; Ripepe et al., 2002), infrasonic (Dalton et al., 2010; Delle Donne et al., 2016; Johnson and Ripepe, 2011; Marchetti et al., 2009), thermal (Patrick et al., 2007; Ripepe et al., 2002), and gas-derived (McGonigle et al., 2009; Pering et al., 2015; Pering et al., 2016; Tamburello et al., 2012) data. Here, we focus on gas emission rate measurements, using the ultraviolet (UV) camera, an instrument frequently used to quantify gas release from persistently outgassing volcanoes (McGonigle et al., 2017; Pering et al., 2019a). The UV camera is able to resolve rapid fluctuations in the release of sulphur dioxide (SO_2) gas. When the camera is used in tandem with an in-situ multi-component gas analyser

(Multi-GAS) to measure gas ratios within a volcanic plume (Aiuppa et al., 2005; Shinohara et al., 2015), it is possible to estimate the total gas emission rate (Pering et al., 2014). An important parameter with respect to causal mechanisms for strombolian explosions is the ratio of gas released during explosions to that released passively (Barth et al., 2019; Jaupart and Vergniolle, 1988, 1989; Parfitt, 2004; Suckale et al., 2016; Vergniolle and Jaupart, 1986). This 'active' to passive degassing ratio also provides information about conduit fluid dynamics (Gaudin et al., 2017a, 2017b; Pering et al., 2015; Pering et al., 2016). For example, Tamburello et al., (2012) discovered that the most efficient mode of degassing at Stromboli was actually the passive degassing, supplying ~77% of gases released, demonstrating the dominance of passive gas release (Carn et al., 2017) and the smaller gas bubbles within a volcanic conduit.

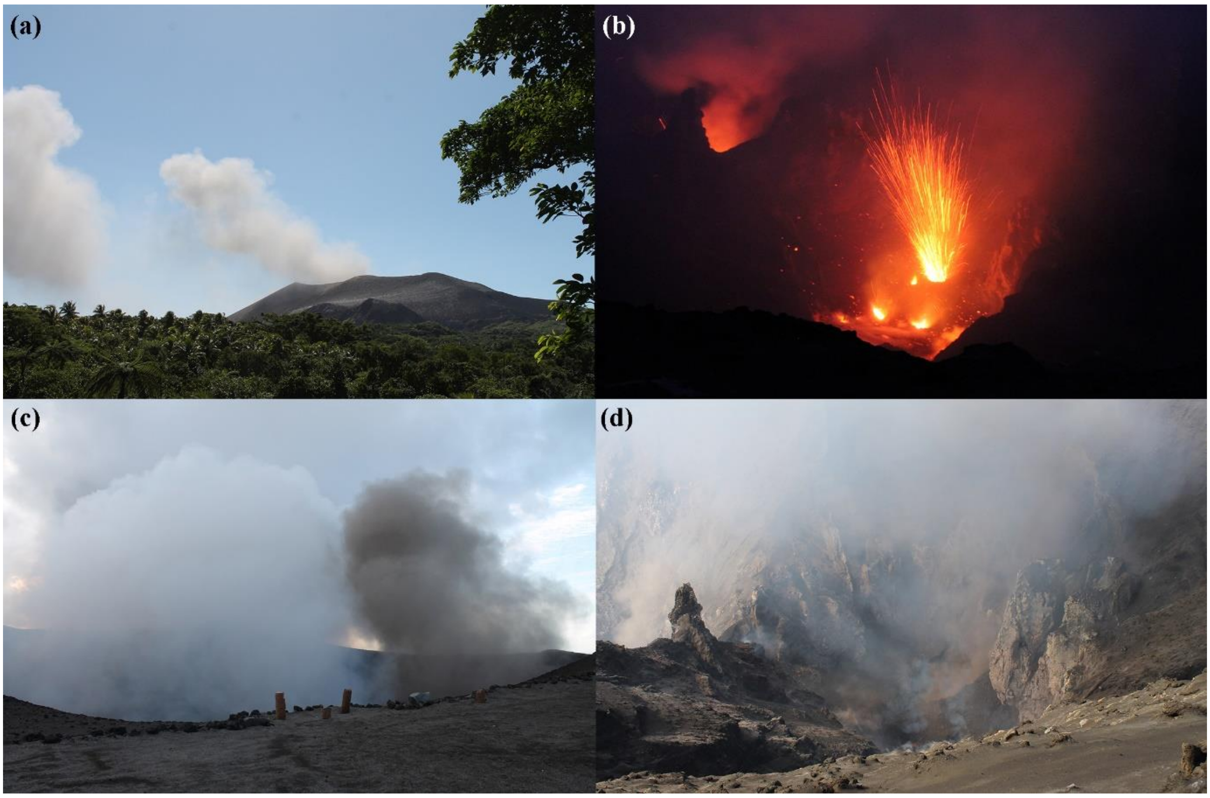

Figure 1: Activity at Yasur Volcano, Vanuatu, during the July 2018 field campaign. (a) Image of the gas plume rising from the summit crater. Large gas pulses are associated with explosions; (b) a night-time view with the south crater in the foreground and incandescence from the north crater in the background. Several vents are visible in the south crater with one producing a strombolian explosion; (c) ash-rich gas plumes formed by strombolian explosions occurred from the north crater and ash-poor gas plumes from explosions from the south crater; (d) a day-time view into the north crater, showing the crater floor topography divided by a septum into northern and southern craters.

UV camera derived SO_2 masses from strombolian explosions (Delle Donne et al., 2016; Mori and Burton, 2009; Pering et al., 2015; Tamburello et al., 2012) can be combined with gas ratio data (e.g., from Multi-GAS), to generate total gas masses and volumes for individual explosive events (Burton et al., 2007; Pering et al., 2016). These data provide parameters for analytical and computational models of gas flow in conduits, which yield further information about the activity and mechanisms; for example, slug length, explosive vigour, and categorisation of burst behaviour using fluid dynamics (Del Bello et al., 2012; James et al., 2009, 2008; Pering and McGonigle, 2018).

Here, we demonstrate the use of a portable, solar-chargeable, version of the low-cost Raspberry Pi ultraviolet camera (Wilkes et al., 2017, 2016) combined with a new approach to estimate plume velocity using UV camera imagery to obtain SO_2 fluxes. We present the first UV camera measurements at Yasur, providing the first gas-based estimate of explosive strombolian gas masses, key to unravelling information on the spectrum of behaviours on this style of activity globally. Furthermore, we illustrate the use of statistical methods to differentiate between passive and explosive gas release, and finally apply mathematical models to estimate driving slug dimensions of the strombolian explosions at Yasur volcano.

2. Yasur volcano and observed activity during 5th to 11th July 2018

Yasur (Vanuatu) is a basaltic stratovolcano, located on the southeast of Tanna Island, which is thought to have been predominantly persistently active for at least ~800 years (Firth et al., 2014). The main volcanic edifice is a cone with a crater area of 350-450 m diameter, divided by a septum into northern and southern craters, each containing multiple active vents. During the measurement period an ashy plume was present throughout the week, related to ash-rich strombolian explosions arising from both craters (Fig 1). From the summit, multiple vents displaying incandescence were visible within the southern crater, each exhibiting different styles of explosive behaviour (Fig 1c). Gas release from the summit vents was constantly visible, occasionally including 'puffing' (described elsewhere by Gaudin et al., 2017b, 2017a; Pering and McGonigle, 2018; Tamburello et al., 2012). The northern crater contained at least two vents, but access to its rim was precluded by safety concerns, due to ballistic ejecta from the crater's strombolian explosions, which also appeared to be more ash-rich than those from the southern crater. From the southern crater (Fig 1d) we directly observed explosions from at least three vents, each of which had different behaviours, two with jet-like characteristics (i.e., with a strong vertical component to the trajectory of ejecta), hinting at the potential influence of the conduit wall during the explosion process, i.e., the explosion (slug burst) happens deeper within the conduit, providing a vertical direction to the released material (Delle Donne and Ripepe, 2012; Salvatore et al., 2020). Another vent exhibited parabolic transport of incandescent pyroclasts (without initial jet), as though an ascending bubble burst within an over-topped magma column (Del Bello et al., 2012), or within a flared conduit geometry (Dibble et al., 2008), i.e., allowing the lateral expansion of bubble prior to burst. Interestingly these strombolian explosions also differed in the noise generated, with the hemispherical shaped (non-jet-like) explosions associated with a deeper booming sound. During 8 – 9 July, explosions were frequently associated with visible shockwaves propagating through the condensed plume. The supplementary video highlights a snapshot of typical activity captured from the both craters. Throughout the measurement period, the morphology of the crater was dynamic, with spatter and ash accumulating around vents leading to changes in the size, shape, and position of vents.

A number of studies on Yasur have focused on the characteristics of strombolian activity and, in particular, its dynamism. Multi-vent basaltic volcanoes are known to exhibit vent-specific behaviours which can change through time, e.g., as shown by Salvatore et al. (2018) on Stromboli. Simons et al., (2020) discuss systematic changes in behaviour at individual vents within the southern crater at Yasur, with switching from bomb-rich (incandescent pyroclasts) through to ash-rich explosions. They also discuss conduit branching and the possibility of a single bubble (i.e., gas slug) driving paired explosions from separate vents at Yasur, with the potential for eruption styles to diverge at different vents due to cooling of the magma in the upper conduit branches. La Spina et al., (2016) observed two decoupled styles of degassing from infrasound data: puffing, which was near-constant, and strombolian explosions. Meier et al., (2016) highlighted the ash-rich and ash-poor (or bomb-rich), styles and their similarity at Yasur to those of Stromboli (Gaudin et al., 2014b; Patrick et al., 2007; Ripepe et al., 2005; Ripepe and Marchetti, 2002; Taddeucci et al., 2012). Kremers et al. (2013) were able to calculate the lengths of gas slugs generating the strombolian explosions on Yasur as ranging from 59 to 244 m, with mean and median values of 112 m and 103 m respectively.

SO_2 fluxes at Yasur ranged from 2.5 to 17.2 kg s^{-1} from April 2004 to November 2005, with a mean of 7.9 kg s^{-1} based on differential optical absorption spectroscopy (DOAS) traverses (Bani and Lardy, 2007). Between August 2007 and December 2008, SO_2 fluxes at Yasur were 1.3 to 11.1 kg s^{-1}, with a mean and median of 7.2 kg s^{-1} and 7.1 kg s^{-1} respectively (Bani et al., 2012). In October 2007, a mean SO_2 flux of 8.0 ± 3.8 kg s^{-1} across four days of traverses was reported by Métrich et al. (2011). A satellite-derived SO_2 flux of 6.8 to 23.3 kg s^{-1} was estimated between 2000-2015, with a mean and median of 16.3 kg s^{-1} and 19.2 kg s^{-1} respectively (Carn et al., 2017). Comparisons in gas flux between different periods of observations and between methods must be treated with caution; they may, in discrete campaigns such as presented in this study, not represent broader changes through time.

3. UV camera methods

Low-cost Raspberry Pi ultraviolet (UV) camera systems ('PiCams') were used to measure volcanic SO_2 outgassing, (Wilkes et al., 2017, 2016); in this case the units were modified to include 'PiJuice' hardware and software (https://github.com/PiSupply/PiJuice) to provide power to the Raspberry Pi boards at the heart of the camera system, see also (Pering et al., 2020). The PiJuice units provide continuous supplies of power via lithium-polymer mobile phone batteries, which can be recharged using solar panels. In the field, both 1600 mAh and 2300 mAh batteries were used. With continuous solar charging (via 40 W solar panels for each Pi board) this configuration readily enabled field data acquisition for at least 6 to 7 hours per day in this location. This camera setup omitted the GPS module in the prior generation of the PiCam system, which automatically provided time synchronisation for the Raspberry Pi computers on start-up. Instead, GPS time synchronisation was performed manually via the command line, expedited by the PiJuices' on board real-time-clocks. The PiCam systems were equipped with two Edmund Optics Inc. filters (of full width at half maximum - 10 nm), centred around 310 and 330 nm, respectively, one for each lens, corresponding to spectral regions where SO_2 does and does not absorb incident UV radiation. As detailed further elsewhere, UV imaging systems in volcanic gas monitoring are predicated upon contrasting image intensities in these two wavebands, to isolate absorption in the image cause by sulphur dioxide absorption; for further details please see: (Gliß et al., 2017; Kantzas et al., 2010; Kern et al., 2015; McGonigle et al., 2017; Mori and Burton, 2006; Platt et al., 2015).

Two separate PiCams (Camera 1 and Camera 2) were operated simultaneously (enabling assessment of error and comparison of two plume angles), viewing the plume from a position southwest of the summit crater from the Treehouse Site (~1900 m from the plume) at the Jungle Oasis, on 6th and 7th July, and from the Ash Plain Site (~2300 m from the plume) to the north-northwest on 8th and 9th July (see Figure 2 for locations). The UV cameras were also operated on the 11th July, however, inclement weather and grounding of the plume prevented reliable data processing for that day. During the measurement days, the plume direction varied from west to northwest, with dry and predominantly cloud-free weather (bar a brief period of rain on 9 July). Of the five days on which measurements were attempted, we acquired high-quality data on four of the days, amassing 16 hours of imagery across these days.

The camera images were captured with acquisition rates of 0.5 – 0.25 Hz, with additional collection of clear sky images prior to the plume sequences' capture, which are required in the processing routine to account for vignetting effects. Dark images were acquired per sequence too, to enable subtraction of dark noise. We conducted frequent calibrations using gas cells with known SO_2 column densities (0 ppm m, 412 ppm m, and 1613 ppm m, with a manufacturer quoted error of 10%) between measurement sequences at least every 1-1.5 hours, with more frequent calibration when light conditions changed more rapidly. The data were then processed following the commonly applied protocols, already extensively described in the literature (D'Aleo et al., 2016; Kantzas et al., 2010; Kern et al., 2014; McGonigle et al., 2017), i.e., aligning images; selecting a clear sky background region; and choosing a plume cross-section along which to determine integrated column amounts (ICA), before multiplying by plume speed to calculate flux. For the resulting flux data time series, we determined data distribution statistically with the Kolmogorov-Smirnov normality test to inform on appropriate measures of central tendency. The data were all non-normally distributed, therefore the median was used in the further calculations, detailed below. However, we continue to detail both mean and median values.

A goal of this study was to attempt to differentiate degassing fluxes from each of the vents. However, it was not possible to do this rigorously and at all times, given that changes in wind shear and crater-derived eddying led to time-varying separation/overlap of individual plumes (Pering et al., 2019b; Tamburello et al., 2013), creating difficulties in resolving emissions from the individual vents. Indeed, the plume predominantly appeared well-mixed on emergence from the summit crater (Figure 2c). However, at times, the view from the Ash Plain Site did allow us to identify gas pulses from two distinct sources, likely corresponding to the two craters, associated with explosions, where distinct gas pulses could be spatially resolved (Figure 2d).

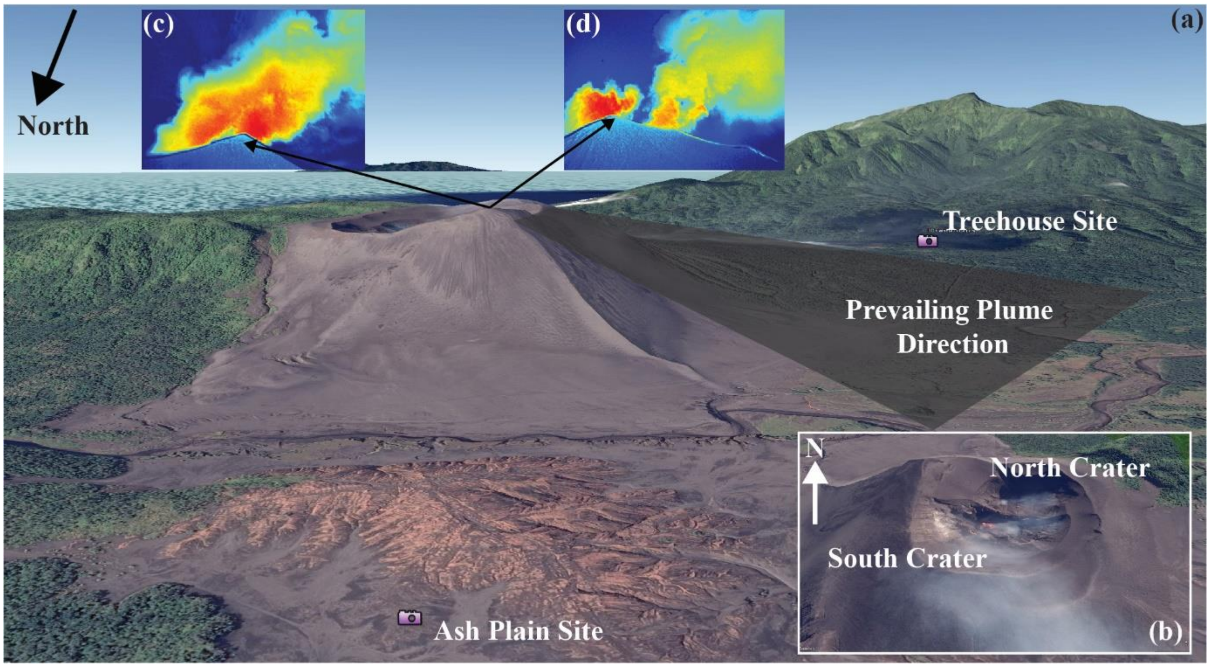

Figure 2: (a) An elevation-based perspective of the low summit of Yasur volcano, along with measurement positions and prevailing plume transport direction with inset (b) showing a close-up of the summit crater. In (c) there is a typical view of the plume with red colours representing higher concentrations of SO_2 showing clear mixing between plumes from different vents, and (d) shows an example of where it was possible to differentiate between emissions from both craters. Imagery is from Google Earth®.

3.1. Particle Image Velocimetry (PIV) for plume velocity determination.

One of the most significant, and yet frequently overlooked, errors in UV camera image analysis is that associated with plume velocity determination, for which three main methods are commonly used: cross-correlation (McGonigle et al., 2005; Williams-Jones et al., 2006), optical-flow (Delle Donne et al., 2019, 2017; Gliß et al., 2017; Kern et al., 2015; Peters et al., 2015; Peters and Oppenheimer, 2018), and manual tracking (Ilanko et al., 2019). The optimal method will largely be determined by the plume conditions, as no single method is ideally suited to all situations. Manual tracking is suitable for stable plumes travelling at slow velocities, or for measurements at greater distances from the plume, where cross-correlation and optical-flow are less desirable, as the plume is more dilute and fewer pixels containing SO_2 are available for the analysis. Cross-correlation is preferred for broadly homogenous plumes that are well-mixed and undergo little turbulence (e.g., whereby eddying can cause SO_2 within parts of the plume to travel backwards relative to the bulk plume vector of motion e.g., the wind direction). Optical-flow methods are well suited to high velocity plumes, where the velocity field over the plume profile is non-constant, e.g., due to pulsed gas outputs from craters, associated with strombolian explosions or puffing (Delle Donne et al., 2019, 2017; Liu et al., 2019; Peters et al., 2015).

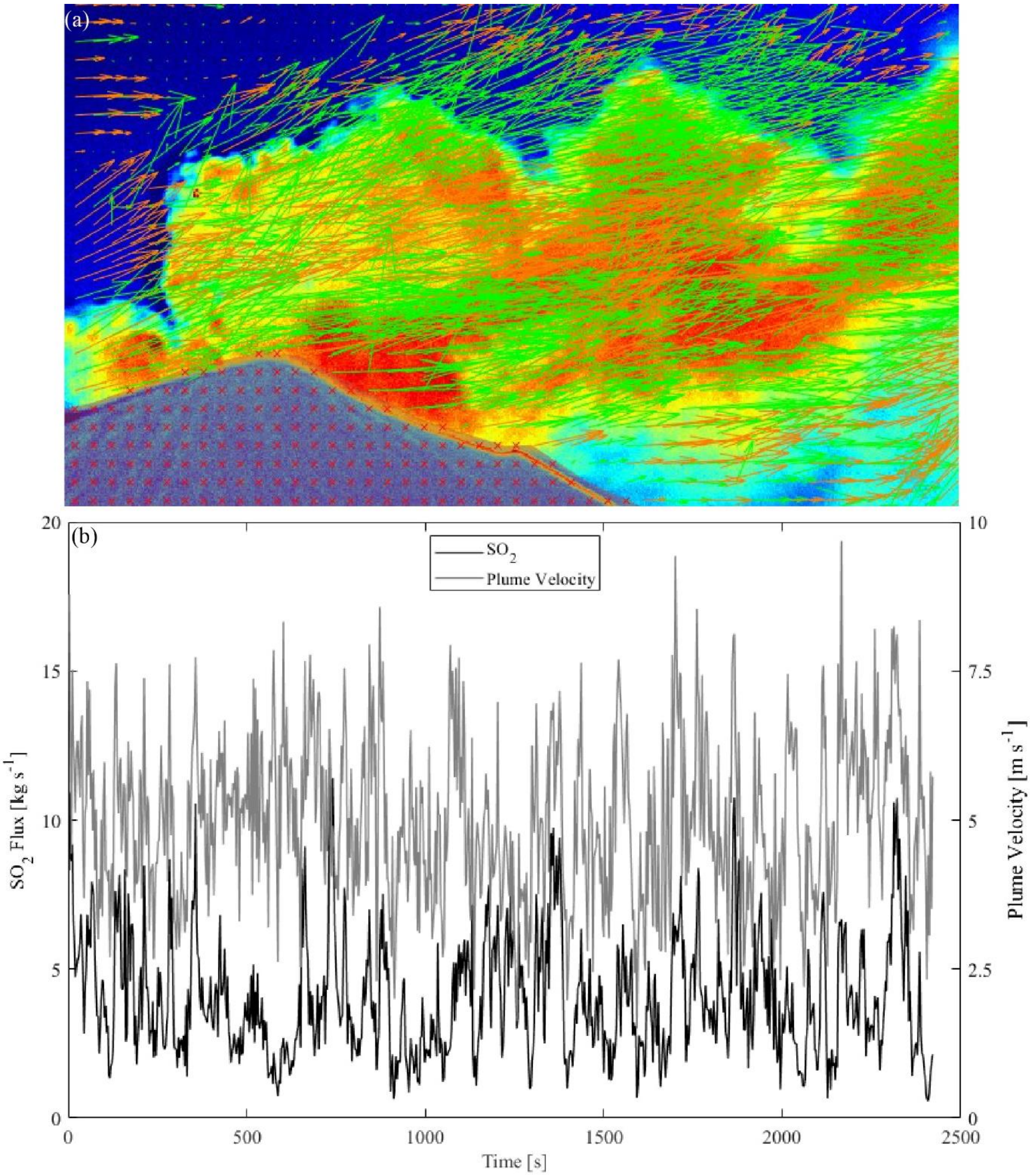

Figure 3: (a) example plume vectors generated during PIV analysis for movement from one frame to the next, superimposed over an SO_2 absorption image; and (b) **e**xample median plume velocity across the integration line and SO_2 fluxes for a time interval of 2500 seconds on 7 July 2018, showing clear accelerations in plume velocities during strombolian explosions.

In this study, we encountered difficulties in using these traditional methods. In particular, efficient mechanisms for tracking pulses of gas in a large dataset were required. Indeed, cross-correlation (which tracks the delay time between two integration lines of known distances) sometimes failed, likely as a result of turbulent motion in the plume. Furthermore this approach does not cope well with the transient increases in gas velocity associated with impulsive gas release during strombolian explosions; hence, this method is probably the least favourable in this context. A lack of structure in the plume appeared to lead to the failure of the Farneback optical flow algorithm (Gliß et al., 2017; Peters et al., 2015; Wilkes et al., 2017). We therefore instead adopted the use of Particle Image Velocimetry (PIV) for plume velocity determination, as briefly discussed in Kern et al., (2014). Previous use of PIV in a volcanic context has included tracking of lava lake velocity at Masaya (Pering et al. 2019) and it is similar to the pyroclast tracking velocimetry of (Gaudin et al., 2014a, 2014b). Here, we used PIVlab, a user-friendly MATLAB toolbox and app (Thielicke, 2014; Thielicke and Stamhuis, 2014). PIV works by comparing image pairs in sequences and looking for differences between them through two methods: direct cross-correlation and through the correlation of Fourier transforms. Both of these methods are conducted on integration areas (here we used three), with decreasing size on each pass. The end result is a velocity grid for the whole plume image, similar to those produced during the application of optical flow (Gliß et al., 2017; Peters et al., 2015), see Figure 3a.

We found that using PIV we were able to detect velocity differences in even the more homogenous plumes (i.e., with a quasi-uniform SO_2 distribution across most of the plume, except during strombolian explosions). PIV was used to extract velocity components corresponding to each image pixel perpendicular to the integration line used in the ICA determination. In this case, rather than using a single plume speed perpendicular to the integration line, therefore, the plume velocity vectors per pixel were multiplied by the pixel's SO_2 column amount, and these ICAs per-pixel were then summed over the plume profile (see Figure 3). The PIV analyses show temporal and spatial variability in plume velocity, capturing a heterogeneity which is a real feature of the plume motion, yet not captured by cross-correlation or manual tracking. We report error for PIV analysis as the length of the integration line at given distance to the plume , corresponding to each pixel, divided by the lowest image capture frequency; for the Ash Plain Site this equates to an error of 2 ± 0.3 ms^{-1} or ~ ±15%, and for the Treehouse Site an error of 5 ± 0.6 ms^{-1} or ~9±%. These error estimates are based on typical plume speeds for each site.

3.2. Estimation of a total UV camera measurement error

Here, we highlight the range of possible error sources, and perform additional analyses on our data pertaining specifically to calibration curve drift, plume orientation, and plume distance. The final determined values for error are our best possible estimates on the basis of the available information and protocols applied in-the-field, which, wherever possible, were designed to minimise error.

The effects of light dilution have been quantified at a range of volcanic gas plume targets: SO_2 mass column amounts may be underestimated by ~10-60% over a range of distances (2.1 km to 6.5 km) and conditions from hazy through to very clear (Campion et al., 2015). Light dilution has a larger effect during hazier conditions, which were not present during our successful measurement days. Ilanko et al., (2019), calculated that at ~10.3 km distance from the plume (during clear conditions at Sabancaya volcano, Peru) SO_2 fluxes could be underestimated by 2.5 times, and at 4.25 km by 1.5 times (which would correspond to ~1.18 times [18%] at our maximum distance of 2300 m at Yasur). It is important to note that light dilution estimates are very specific to each measurement location and conditions, and given our range of distances to the plume and clear measurement conditions we suggest therefore that error relating to light dilution is <+20%. We also note that the plume was not optically thick, except following ash-rich strombolian explosions. Unfortunately, exact errors due to scattering of UV by ash are currently not quantifiable, but ash within the plume will likely lead to an underestimation of SO_2 column amounts (Kern et al., 2013; Tamburello et al., 2012).We attempted to minimise this error by integrating away from the summit area, where the plume is visibly less ash-rich, and more transparent. We also further note that the peaks in gas flux from strombolian explosions are well defined within the resulting dataset (Figure 3).

Table 1: A summary of errors on UV camera measurements of SO_2 fluxes at Yasur Volcano in July 2018, including short comments and total RMS error.

	Treehouse	**Ash Plain**	**Comments**
Distance	1900 m	2300 m	-
Description	**Error**	**Error**	-
Light Dilution	+20%	+20%	Underestimation only, low given plume proximity.
Gas Cell Concentration	±10%	±10%	Manufacturer quoted
Calibration drift	±15%	±15%	Changing calibration conditions (see text)
Plume Velocity	±9	±15%	Based on pixel size (see text)
Plume Direction	±5%	±5%	Based on coincident UV camera data
Plume Distance	±18%	±18%	Based on plume deviation of 200 m.
Ash content	-	-	Underestimation, not quantifiable
RMS Error	-11.2% / +13.9%	-12.2% / +14.7%	Note the higher error related to underestimation (positive error).

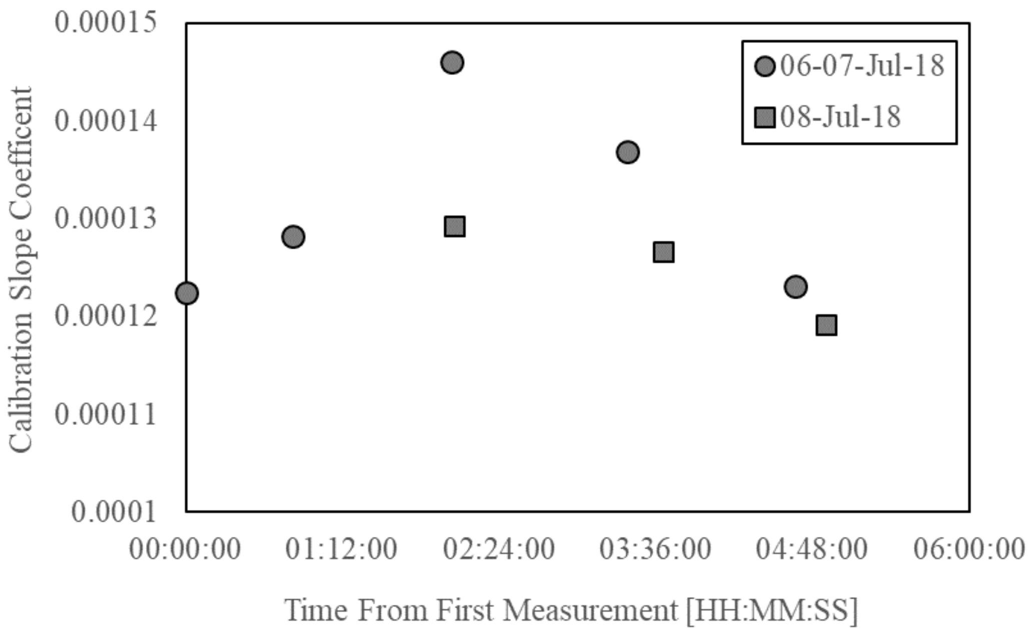

Figure 4: Example calibration slope coefficients (derived from regressions of gas cell concentrations against apparent absorbance) from two days of data. Timings are from the time of the first calibration on each of these measurement days. Note that the coefficient peaks towards solar noon.

Gas cell calibrations change throughout the day in response to position of the sun and changing illumination as a result of background clouds, with changes in gas-cell calibrations potentially leading to over-estimation in SO_2 column densities of up to 60% (Lübcke et al., 2013). Figure 4 shows the change in calibration slope coefficient (between regressions of apparent absorbance coefficient and column density) throughout the day from time of first calibration (rather than using UTC), showing a variation from 1.22×10^{-4} to 1.46×10^{-4} in this parameter. When taking into account this characterised range in slope of 2.4×10^{-5}, and the broad assumption (for indicative purposes) that there is a linear change between the first point and the highest point (corresponding to maximum solar zenith angle) we arrive, over the 122 minutes between these points, at a value of 1.97×10^{-7} increase in slope coefficient per minute. This would equate to a potential change in error of ~ 0.16% per minute, which expanded over an hour could become 9.6% - or, for our maximum inter-calibration interval of ~95 minutes, an error of 15.2%. It is possible therefore that any underlying trends in apparent gas emission rates below these thresholds are not differentiable from this error, i.e., an increase or decrease in flux at a rate of <~0.16% per minute. We suggest therefore that errors from cell calibration (notwithstanding the ~±10% manufacturer quoted cell content error) amount to a maximum of ±15% for our measurement period.

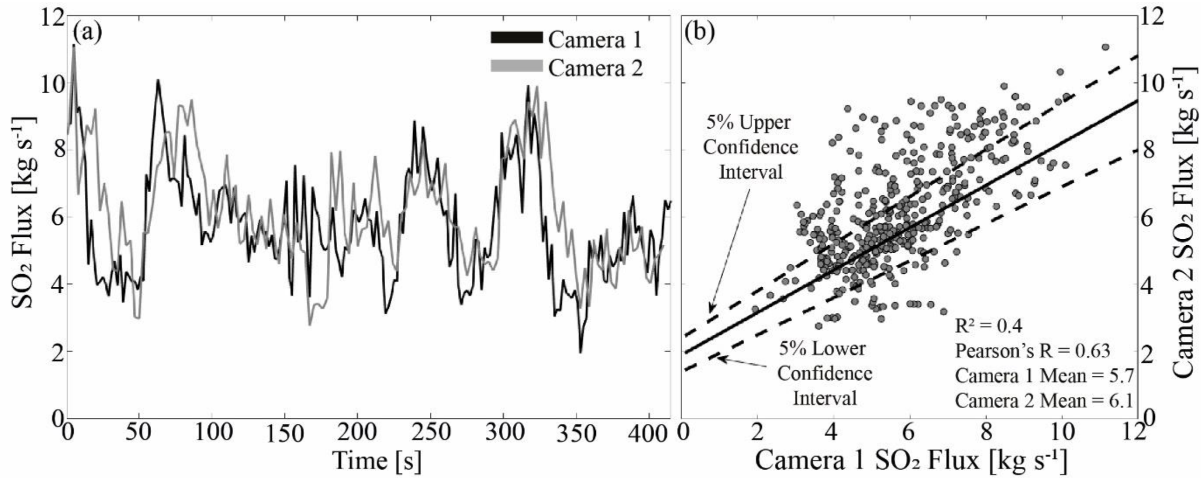

Figure 5: (a) Example period of overlapping data from two separately acquiring synchronous cameras, viewing the plume from slightly different orientations. One dataset has been shifted by the lag value which generated the maximum correlation coefficient, following cross-correlation between the two series, in an attempt to best temporally match the data. Note that there are differences in the magnitudes of peaks and troughs in the different dataseries, even when shifted relative to one another in this way, due to smoothing or turbulence during plume movement through the atmosphere and the slightly different views of the units through the plume. In (b) a linear regression model ($R^2 = 0.4$) is shown, demonstrating the best fit between time series data from the two cameras, as well as confidence intervals. The statistical parameters are similar, but there are differences in peaks and troughs between the two datasets.

We used fixed distances of 1900 m and 2300 m from the camera to the plume for our retrieval calculations in the cases of data from the Treehouse and Ash Plain Sites respectively. By repeating the same retrievals at different distances, for the Ash Plain data, we determined that a 100 m error in plume distance leads to a < 5% difference in computed gas masses across the plume cross section (with underestimation in this distance corresponding to underestimation in gas mass), and a 200 m error in distance to < 9% error. Comparisons of the same test dataset with different velocities in PIV analyses corresponding to the different distances showed variations from 1 – 7 % with the 100 m error and 5 – 11% in the 200 m case. The combined effect of distance uncertainties on mass and velocity gives a 7-10% error in fluxes for 100 m distance to plume error, and 16-18 % for 200 m. We therefore take the maximum value here of ~18% and apply this conservatively, to our entire dataset.

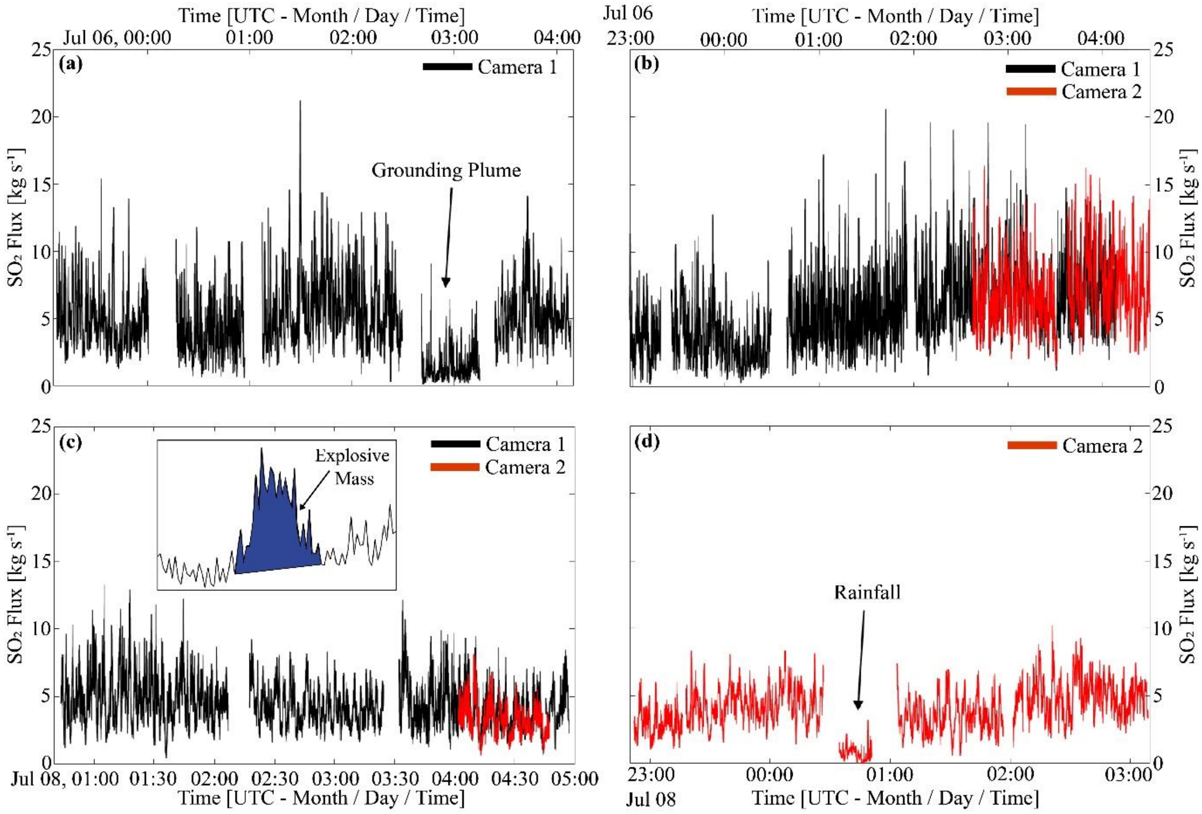

Figure 6: (a) through (d) show retrieved gas fluxes, where clear peaks correspond to strombolian explosions, for all the image data captured during the observation period; also highlighted are periods where the plume was grounded in (a) and heavy rainfall was encountered in (d). Inset in (c) is an example of explosive mass determination, where integration occurs below the explosion peak (e.g., shaded blue area), above background levels.

Given changes in plume direction, the orientation with which the integration line bisects the plume is also relevant in consideration of measurement uncertainty (Klein et al., 2017). To investigate this, we use overlaps between data from two synchronously-acquiring cameras (Figure 5), which had slightly different plume views and hence integration line orientations relative to the plume geometry. This simulates the time-dependent effect of the plume moving, in response to changing wind conditions, with respect to a fixed integrated column amount line. In this case the two datasets were cross-correlated and shifted by the lag corresponding to the maximum correlation to account for different transport times from the source to the two cameras' different integration lines. The calculated difference in flux retrieval from the two units, based on comparing the acquired median values per unit is ~±5%.

In addition, we also report computed flux data in Figure 6 (which documents the retrieved data from the entire campaign) during periods when the plume grounded, e.g., the integration line could not cover the entire plume cross section, as well as episodes of heavy rainfall. During these periods, median SO_2 fluxes were underestimated significantly by ~4.3-4.4 and 5.6-7.3 times, respectively, based on comparison with median values of retrieved fluxes either side of these episodes. Whilst the data captured under these circumstances were not used in the foregoing analysis, nor considered representative of the volcanic outgassing, they are reported here, to illustrate the significant error to which these effects give rise.

Table 2. A summary of measurement durations and SO_2 flux statistics for daily UV camera measurements at Yasur Volcano in July 2018.

Date (UTC)	**05-06/07/18**	**06-07/07/18**	**08/07/18**	**08-09/07/18**
Date (Local)	**06/07/18**	**07/07/18**	**08/08/18**	**09/08/18**
Time series duration (hh:mm)	4:15	04:42	03:54	03:33
Total time (hh:mm)	05:01	05:31	04:14	04:17
Mean (kg/s)	5.2	5.5	4.5	4.1
Median (kg/s)	4.7	5.1	4.2	4.0

4. Results and Discussion

4.1 SO_2 fluxes and estimates of the masses of gas emitted during strombolian explosions

Time series gas fluxes are shown in Figure 6, with a summary of daily statistics in Table 1. The median flux across the four days of measurements was 4.5 kg s^{-1} and the mean was 4.9 kg s^{-1}, reflecting the peaks in SO_2 flux associated with frequent strombolian explosions. These gas fluxes correspond to a daily median and mean of 389 and 423 t d^{-1} across the measurement period. Daily statistics are given in Table 2: median SO_2 fluxes ranged between 4.0 to 5.1 kg s^{-1} across the measurement days and the daily means were 4.1 to 5.5 kg s^{-1}. The timeseries data are suggestive of gradual changes in background SO_2 emissions over several hours, but it is not clear whether these are real or a product of artefact error. A shift in activity is, however, plausible based on the observation of large strombolian explosions with visible ballistics and shockwaves, particularly on 8 and 9 July, when lower fluxes were measured.

Masses of SO_2 released during each strombolian explosion were calculated by integrating beneath the explosive pulse and summing the total SO_2 released, after Tamburello *et al.*, (2012), see Figure 6c. However, a challenge here is that the onsets of strombolian explosions were not visible within the imagery (i.e., vents were at depth within the crater). We use two methods to determine when explosions occurred within the UV camera imagery: firstly, gas pulses in the camera images must be observed to originate and visibly accelerate above the rim of the summit crater (see Figure 1a) to confirm that an explosion occurred; secondly, where gas burst traces are manifested in the flux time series, showing the characteristic coda (a period of elevated flux following a strombolian explosions which gradually declines) detailed in Pering et al., (2016), see Figure 6c. The number of explosions is probably underestimated using these methods; however, the resulting estimation of SO_2 released during each explosion is useful for comparison to literature values (Table 3). Overall, SO_2 masses released were estimated for 135 explosions, across five days. Mean masses of SO_2 released increased from 6th to 9th July 2018, which is consistent with visual observations of more powerful explosions on 8 and 9 July 2018.

Table 3: A breakdown of daily SO_2 explosion mass data. Also displayed are percentages indicating the partitioning of gas masses between passive and explosive degassing. Lower and Upper -ratios refer to the ranges indicated in determined active molar ratios by (Woitischek et

al., 2020; Table 3 - $CO_2/SO_2 = 2.85 \pm 0.17$; $H_2O/SO_2 = 315 \pm 71.8$; $SO_2/HCl = 1.6 \pm 0.22$). [1] These values are from the statistical calculation of this paper (section 4.2).

Date (UTC)	**05/07/2018**	**06/07/2018**	**07/07/2018**	**08/07/2018**	**09/07/2019**	**Total**
Explosions Counted	8	43	39	36	9	**135**
						Mean
SO_2 Min (kg)	10.2	8.9	8	12	10	**9.8**
SO_2 Mean (kg)	26.9	22.1	27	39	45	**32.0**
SO_2 Max (kg)	64.1	44.9	62	81	69	**64.2**
Passive[1] %	66	64	70	78	68	**69**
Explosive[1] %	34	36	30	22	32	**31**
Masses from Lower Ratios						
Total – Min (kg)	712	625	575	822	721	**691**
Total – Mean (kg)	1884	1550	1892	2713	3164	**2241**
Total – Max (kg)	3020	3148	4370	5678	4813	**4206**
Masses from Mean Ratios						
Total – Min (kg)	940	824	759	1084	952	**912**
Total – Mean (kg)	2486	2046	2497	3579	4175	**2957**
Total – Max (kg)	5929	4153	5767	7493	6350	**5938**
Masses from Upper Ratios						
Total – Min (kg)	1167	1024	942	1347	1182	**1132**
Total – Mean (kg)	3088	2541	3102	4446	5186	**3673**
Total – Max (kg)	7365	5159	7163	9307	7888	**7376**

The range of SO_2 masses released during strombolian explosions at Yasur, of 8 – 69 kg (mean 32 kg) are similar to those estimated by Tamburello et al., (2012) at Stromboli, who found a range of 2 – 55 kg (mean of 20 kg); but higher than those observed at Etna during mild strombolian activity (Pering et al., 2015), which ranged from 0.1 to 14 kg. Gas ratios (SO_2, H_2S, H_2O and CO_2) derived from a combined Fourier transform infrared spectroscopy (FTIR) and Multi-GAS study from 6 to 16 July 2018 show distinct gas compositions during passive and explosive activity (Woitischek et al., 2020). Gas emitted during active (strombolian) activity had molar ratios of: $CO_2/SO_2 = 2.85 \pm 0.17$; $H_2O/SO_2 = 315 \pm 71.8$; $SO_2/HCl = 1.7 \pm 0.22$. Using these data we can estimate total gas slug masses, shown in Table 3. The mean total gas mass emitted during strombolian explosions at Yasur is 2960 kg, with a range of 910 – 5940 kg. These estimates are similar to the 170 – 1674 kg for strombolian explosions at Pacaya (Dalton et al., 2010) whereas at Stromboli, explosion masses range from 44 – 238 kg according to Barnie et al. (2015) and 2 to 1425 kg as determined by Delle Donne et al. (2016).

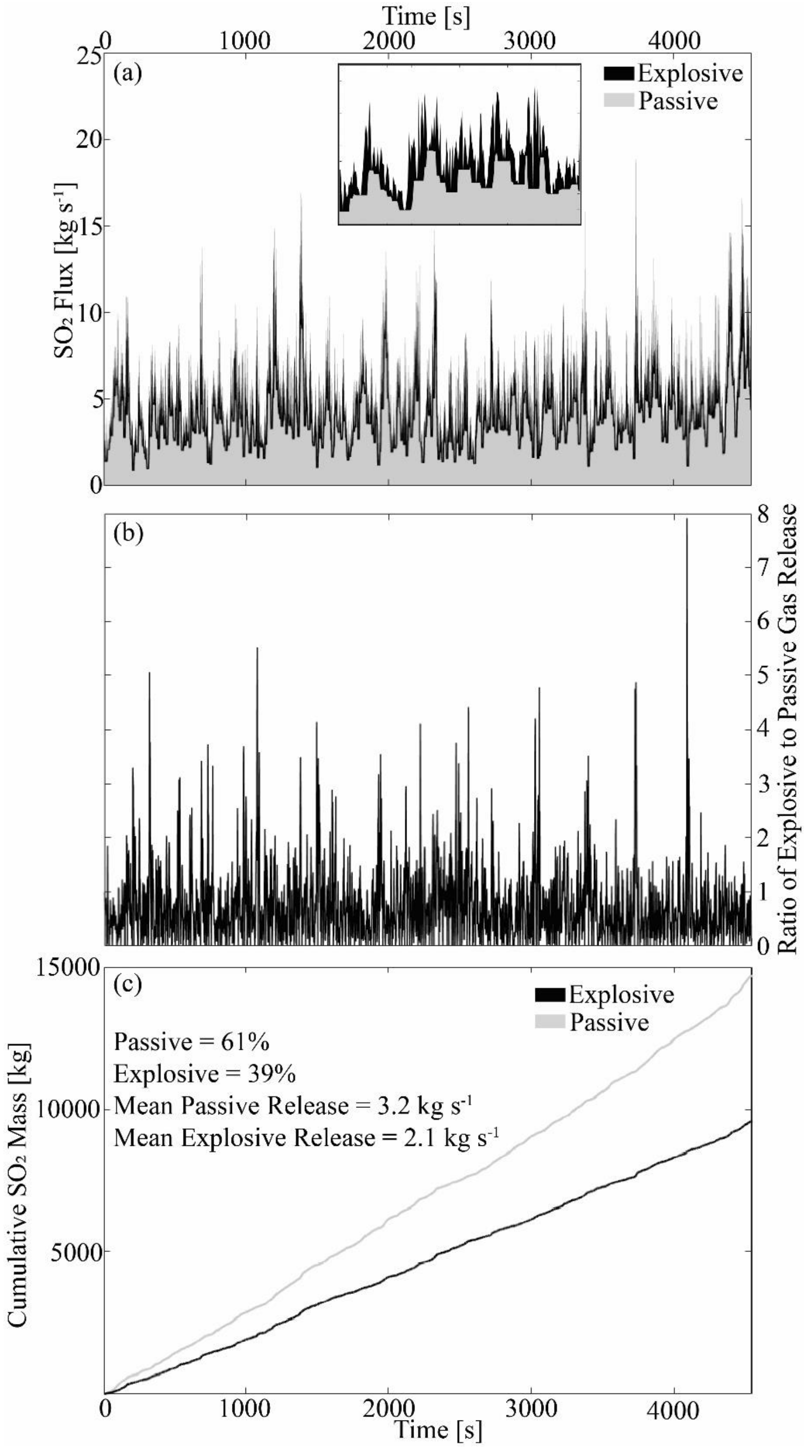

Figure 7: (a) Separation of passive and explosion gas release for a period on the 7th July with (inset) a zoomed illustration of the simple statistical moving minimum based model, showing oscillation in background passive degassing overtopped by explosive contributions; (b) the ratio of passive to explosive degassing; and (c) a cumulative plot showing the division between passive and explosive gas release, here passive and explosive release have been cumulatively summed to show the change through time at the sampling frequency. The passive to explosive ratio is then the ratio of the final sum of gas release.

4.2. Simple Statistical Separation of Passive and Explosive Degassing

Others have studied the ratios of explosive to passive release during strombolian explosions on Stromboli (Tamburello et al., 2012) and Etna (Pering et al., 2015). Here, we attempt to expand on this by using a simple statistical measure involving the moving minimum (which traces the lower values in dataset over a defined window, much as the moving mean), to estimate the passive release of gas through time, which, when subtracted from total flux, provides an approximate estimate of passive vs. explosive release. This was necessary as our manual selection of events missed or excluded several strombolian explosions. Our approach is similar to the automated method of Delle Donne et al., (2017), which involved finding local peaks in timeseries data. For an example period (Figure 7) we highlight the moving minimum, which is set to a window size of 20 s, which is generally the characteristic timeframe of large peaks and troughs associated with strombolian explosions (Delle Donne et al., 2017; Pering et al., 2016). Note that, using this moving minimum method, an oscillation (non-uniform) background is apparent. Delle Donne et al., (2017), also showed fluctuation in passive background between strombolian explosions, and this background is used as a best estimate solely to extract the explosive contribution. In this instance, at Yasur, a moving minimum over this window proved best, given the higher frequency of explosive events; however, with a greater timeframe between events, the moving median may be a better measure. We also prefer this statistical estimation technique over using our estimated SO_2 masses, given that the latter required manual selection of strombolian explosions. This simple moving minimum approach could be readily and simply automated for routine monitoring of activity from strombolian explosion producing volcanic systems.

Daily estimates of the passive and active degassing contributions are shown in Table 3, with a mean of 69% passive to 31% explosive. These estimates are similar to those estimated at Stromboli: 77% passive to 23% explosive (termed active which also includes puffing); and Etna: 67% passive to 33% explosive (Pering et al., 2015). These datasets serve to illustrate the dominance of passive degassing in the gas emission budget at volcanoes that exhibit strombolian activity. On the 8th July 2018 we calculated a higher passive degassing contribution, at 78%. This day was characterised by higher SO_2 masses emitted during individual explosions, but lower overall SO_2 fluxes. These features may be consistent with a degassing magma column beneath a thicker, more viscous and impermeable crystal-rich plug, requiring a higher gas mass to drive more powerful explosions (Polacci et al., 2012; Simons et al., 2020; Woitischek et al. 2020), which is consistent with visual observations.

4.3.Models of gas slug behaviour

Using our determined values for total slug mass, we can estimate slug lengths using the static pressure model of (Del Bello et al., 2012). We use fixed values of 2600 kg m^3 and 1000 Pa s^{-1} for density and viscosity, respectively, with an atmospheric pressure of 101,325 Pa. The only parameter we vary in the model is that of conduit diameter, which we step from 3 m to 7 m. We use only the mean explosive gas ratios and masses (and not the range obtained when including error) for simplicity. It should be noted that the molar H_2O/SO_2 ratio is high and variable (Woitischek et al., 2020). As water is the gas contributing most to the mass of the slug, it is likely that our determined total gas masses are an overestimation. Our results are summarised in Table 4. We determine slug lengths ranging 188 – 609 m (median and mean of 347 m and 366 m respectively) for a conduit diameter of 3 m, however, this reduces to 76 – 260 m (median and mean of 146 and 154 m respectively) for a conduit diameter of 7 m. Kremers et al. (2013) calculated lower values of 59 – 244 m using seismo-acoustic data, and it would therefore seem that a larger conduit diameter may be more plausible at Yasur, which may bifurcate or split at very shallow depths (Simons et al., 2020).

Table 4: A summary of gas slug volumes and lengths using the model of Del Bello et al. (2012) and based on gas flux and composition data acquired during strombolian activity at Yasur Volcano in July 2018.

Statistic	**Slug Volume (m^3)**	**D = 3 m**	**D = 4 m**	**D = 5 m**	**D = 6 m**	**D = 7 m**
Min	4286	188	139	110	90	76
Median	14055	347	259	205	170	146
Mean	15556	366	272	217	180	154
Max	42337	609	455	364	303	260

5. Summary and Conclusions

In this work we highlighted the utility of using low-cost solar-powered Raspberry Pi UV cameras for prolonged field campaigns. We continuously imaged the volcanic plume to yield both velocity, using a PIV method (Thielicke, 2014; Thielicke and Stamhuis, 2014), and SO_2 fluxes over periods of several hours per day, at temporal resolutions of up to 0.5 Hz with brief pauses for calibration. SO_2 fluxes were determined, with daily means of 4.1-5.5 kg s^{-1} (medians from 4.0-5.1 kg s^{-1}) which are within the ranges of those measured previously at Yasur using ground-based methods of 2.5 to 17.2 kg s^{-1} (Bani et al., 2012; Bani and Lardy, 2007). SO_2 masses emitted during individual strombolian explosions ranged from 8-81 kg, similar to events at Stromboli, which were associated with the emission of 2 – 55 kg SO_2 (Tamburello et al., 2012). By using a simple statistical measure we estimate that passive degassing, at 69%, is the dominant mode of degassing at Yasur, compared to 31% explosive. Observations suggest that periods of lower gas output are associated with conduit sealing and more violent explosions, however, a longer dataset would be needed to test this hypothesis substantively. By combining SO_2 explosion masses with gas ratios (Woitischek et al., 2020) we determined total explosion gas masses of mean 910-5940 kg, which correspond to slug lengths, using the model of Del Bello et al. (2012) of 76-260 m, if a larger conduit diameter of 7 m is used. Smaller conduit diameters lead to longer slug lengths ~188-600 m at 3 m diameter, larger than those estimated previously of ~59 – 244 m (Kremers et al., 2013). The data presented here represent an important addition to our gas data based characterisation of the spectrum of strombolian activity across the globe.

6. Acknowledgements

We would like to thank the Vanuatu Meteorology and Geo-hazards Department for permission to conduct this fieldwork, Kelson and Joyce Hosea for their hospitality at the Jungle Oasis, and Roger for his assistance in the field. J.W and M.E .were supported by the Natural Environment Research Council (grant number NE/L002507/1), by the postgraduate travel funds received from Fitzwilliam College, by the Elspeth Matthews grant given by the Royal Geological Society, by the Mary Euphrasia Mosley, Sir Bartle Frere and Worts travel fund report given by the University of Cambridge and by the Exzellenzstipendium received by WKO. A.A. acknowledges funding support from the Alfred P. Sloan Foundation via the Deep Carbon Observatory (UniPa-CiW subcontract 10881-1262) and from MIUR (under grant n. PRIN2017-2017LMNLAW). T.D.P. acknowledges the support of the Royal Society (RG170226). T.I. is a Commonwealth Rutherford Fellow, funded by the UK government. A.McG. acknowledges support from the Rolex Institute.

7. References

Aiuppa, A., Coco, E. Lo, Liuzzo, M., Giudice, G., 2016. Terminal Strombolian activity at Etna's central craters during summer 2012: The most CO_2-rich volcanic gas ever recorded at Mount Etna. Geochem. J. 50, 123–138. https://doi.org//10.2343/geochemj.2.0395

Aiuppa, A., Federico, C., Giudice, G., Gurrieri, S., 2005. Chemical mapping of a fumarolic field: La Fossa Crater, Vulcano Island (Aeolian Islands, Italy). Geophys. Res. Lett. 32, L13309. https://doi.org/10.1029/2005GL023207

Bani, P., Lardy, M., 2007. Sulphur dioxide emission rates from Yasur volcano, Vanuatu archipelago. Geophys. Res. Lett. 34. https://doi.org/10.1029/2007GL030411

Bani, P., Oppenheimer, C., Allard, P., Shinohara, H., Tsanev, V., Carn, S., Lardy, M., Garaebiti, E., 2012. First estimate of volcanic SO_2 budget for Vanuatu island arc. J. Volcanol. Geotherm. Res. 211–212, 36–46. https://doi.org/10.1016/j.jvolgeores.2011.10.005

Barnie, T., Bombrun, M., Burton, M.R., Harris, A., Sawyer, G., 2015. Quantification of gas and solid emissions during Strombolian explosions using simultaneous sulphur dioxide and infrared camera observations. J. Volcanol. Geotherm. Res. 300, 167–174. https://doi.org/10.1016/j.jvolgeores.2014.10.003

Barth, A., Edmonds, M., Woods, A., 2019. Valve-like dynamics of gas flow through a packed crystal mush and cyclic strombolian explosions. Sci. Rep. 9, 821. https://doi.org/10.1038/s41598-018-37013-8

Battaglia, A., Bitetto, M., Aiuppa, A., Rizzo, A.L., Chigna, G., Watson, I.M., D'Aleo, R., Juárez Cacao, F.J., de Moor, M.J., 2018. The Magmatic Gas Signature of Pacaya Volcano, With Implications for the Volcanic CO_2 Flux From Guatemala. Geochemistry, Geophys. Geosystems 19, 667–692. https://doi.org/10.1002/2017GC007238

Blackburn, E.A., Wilson, L., Sparks, R.S.J., 1976. Mechanisms and dynamics of strombolian activity. J. Geol. Soc. London. 132, 429–440. https://doi.org/10.1144/gsjgs.132.4.0429

Branca, S., Del Carlo, P., 2005. Types of eruptions of Etna volcano AD 1670-2003: Implications for short-term eruptive behaviour. Bull. Volcanol. 67, 732–742. https://doi.org/10.1007/s00445-005-0412-z

Burton, M., Allard, P., Mure, F., La Spina, A., 2007. Magmatic Gas Composition Reveals the Source Depth of Slug-Driven Strombolian Explosive Activity. Science (80-.). 317, 227–230. https://doi.org/10.1126/science.1141900

Campion, R., Delgado-Granados, H., Mori, T., 2015. Image-based correction of the light dilution effect for SO2 camera measurements. J. Volcanol. Geotherm. Res. 300, 48–57. https://doi.org/10.1016/j.jvolgeores.2015.01.004
Carn, S.A., Fioletov, V.E., Mclinden, C.A., Li, C., Krotkov, N.A., 2017. A decade of global volcanic SO2 emissions measured from space. Sci. Rep. 7, 1–12. https://doi.org/10.1038/srep44095
Chouet, B., Dawson, P., Ohminato, T., Martini, M., Saccorotti, G., Giudicepietro, F., De Luca, G., Milana, G., Scarpa, R., 2003. Source mechanisms of explosions at Stromboli Volcano, Italy, determined from moment-tensor inversions of very-long-period data. J. Geophys. Res. Solid Earth 108, 2019. https://doi.org/10.1029/2002JB001919
D'Aleo, R., Bitetto, M., Delle Donne, D., Tamburello, G., Battaglia, A., Coltelli, M., Patanè, D., Prestifilippo, M., Sciotto, M., Aiuppa, A., 2016. Spatially resolved SO2 flux emissions from Mt Etna. Geophys. Res. Lett. 43, 7511–7519. https://doi.org/10.1002/2016GL069938
Dalton, M.P., Waite, G.P., Watson, I.M., Nadeau, P.A., 2010. Multiparameter quantification of gas release during weak Strombolian eruptions at Pacaya Volcano, Guatemala. Geophys. Res. Lett. 37. https://doi.org/10.1029/2010GL042617
Del Bello, E., Llewellin, E.W., Taddeucci, J., Scarlato, P., Lane, S.J., 2012. An analytical model for gas overpressure in slug-driven explosions: Insights into Strombolian volcanic eruptions. J. Geophys. Res. Solid Earth 117. https://doi.org/10.1029/2011JB008747
Delle Donne, D., Aiuppa, A., Bitetto, M., D'aleo, R., Coltelli, M., Coppola, D., Pecora, E., Ripepe, M., Tamburello, G., 2019. Changes in SO 2 Flux Regime at Mt. Etna Captured by Automatically Processed Ultraviolet Camera Data. Remote Sens. 11, 1201. https://doi.org/10.3390/rs11101201
Delle Donne, D., Ripepe, M., 2012. High-frame rate thermal imagery of strombolian explosions: Implications for explosive and infrasonic source dynamics. J. Geophys. Res. Solid Earth 117, 1–12. https://doi.org/10.1029/2011JB008987
Delle Donne, D., Ripepe, M., Lacanna, G., Tamburello, G., Bitetto, M., Aiuppa, A., 2016. Gas mass derived by infrasound and UV cameras: Implications for mass flow rate. J. Volcanol. Geotherm. Res. 325, 169–178. https://doi.org/10.1016/j.jvolgeores.2016.06.015
Delle Donne, D., Tamburello, G., Aiuppa, A., Bitetto, M., Lacanna, G., D'Aleo, R., Ripepe, M., 2017. Exploring the explosive-effusive transition using permanent ultraviolet cameras. J. Geophys. Res. Solid Earth 122, 4377–4394. https://doi.org/10.1002/2017JB014027
Dibble, R.R., Kyle, P.R., Rowe, C.A., 2008. Video and seismic observations of Strombolian eruptions at Erebus volcano, Antarctica. J. Volcanol. Geotherm. Res. 177, 619–634. https://doi.org/10.1016/j.jvolgeores.2008.07.020
Firth, C.W., Handley, H.K., Cronin, S.J., Turner, S.P., 2014. The eruptive history and chemical stratigraphy of a post-caldera, steady-state volcano: Yasur, Vanuatu. Bull. Volcanol. 76, 1–23. https://doi.org/10.1007/s00445-014-0837-3
Garcés, M.A., Hagerty, M.T., Schwartz, S.Y., 1998. Magma acoustics and time-varying melt properties at Arenal Volcano, Costa Rica. Geophys. Res. Lett. 25, 2293–2296. https://doi.org/10.1029/98GL01511
Gaudin, D., Moroni, M., Taddeucci, J., Scarlato, P., Shindler, L., 2014a. Pyroclast Tracking Velocimetry: A particle tracking velocimetry-based tool for the study of Strombolian explosive eruptions. J. Geophys. Res. Solid Earth 119, 5369–5383. https://doi.org/10.1002/2014JB011095
Gaudin, D., Taddeucci, J., Scarlato, P., del Bello, E., Ricci, T., Orr, T., Houghton, B., Harris, A., Rao, S., Bucci, A., 2017a. Integrating puffing and explosions in a general scheme for

Strombolian-style activity. J. Geophys. Res. Solid Earth 122, 1860–1875. https://doi.org/10.1002/2016JB013707
Gaudin, D., Taddeucci, J., Scarlato, P., Harris, A., Bombrun, M., Del Bello, E., Ricci, T., 2017b. Characteristics of puffing activity revealed by ground-based, thermal infrared imaging: the example of Stromboli Volcano (Italy). Bull. Volcanol. 79, 24. https://doi.org/10.1007/s00445-017-1108-x
Gaudin, D., Taddeucci, J., Scarlato, P., Moroni, M., Freda, C., Gaeta, M., Palladino, D.M., 2014b. Pyroclast Tracking Velocimetry illuminates bomb ejection and explosion dynamics at Stromboli (Italy) and Yasur (Vanuatu) volcanoes. J. Geophys. Res. Solid Earth 119, 5384–5397. https://doi.org/10.1002/2014JB011096
Gliß, J., Stebel, K., Kylling, A., Dinger, A., Sihler, H., Sudbø, A., Gliß, J., Stebel, K., Kylling, A., Dinger, A.S., Sihler, H., Sudbø, A., 2017. Pyplis–A Python Software Toolbox for the Analysis of SO2 Camera Images for Emission Rate Retrievals from Point Sources. Geosciences 7, 134. https://doi.org/10.3390/geosciences7040134
Ilanko, T., Oppenheimer, C., Burgisser, A., Kyle, P., 2015. Transient degassing events at the lava lake of Erebus volcano, Antarctica: Chemistry and mechanisms. GeoResJ 7, 43–58. https://doi.org/10.1016/j.grj.2015.05.001
Ilanko, T., Pering, T., Wilkes, T., Apaza Choquehuayta, F., Kern, C., Díaz Moreno, A., De Angelis, S., Layana, S., Rojas, F., Aguilera, F., Vasconez, F., McGonigle, A., 2019. Degassing at Sabancaya volcano measured by UV cameras and the NOVAC network. Volcanica 2, 239–252. https://doi.org/10.30909/vol.02.02.239252
James, M.R., Lane, S.J., Corder, S.B., 2008. Modelling the rapid near-surface expansion of gas slugs in low-viscosity magmas. Geol. Soc. London, Spec. Publ. 307, 147–167. https://doi.org/10.1144/GSL.SP.2003.213.01.17
James, M.R., Lane, S.J., Wilson, L., Corder, S.B., 2009. Degassing at low magma-viscosity volcanoes: Quantifying the transition between passive bubble-burst and Strombolian eruption. J. Volcanol. Geotherm. Res. 180, 81–88. https://doi.org/10.1016/j.jvolgeores.2008.09.002
Jaupart, C., Vergniolle, S., 1989. The generation and collapse of a foam layer at the roof of a basaltic magma chamber. J. Fluid Mech. 203, 347–380. https://doi.org/10.1017/S0022112089001497
Jaupart, C., Vergniolle, S., 1988. Laboratory models of Hawaiian and Strombolian eruptions. Nature 331, 58–60. https://doi.org/10.1038/331058a0
Johnson, J.B., Aster, R.C., 2005. Relative partitioning of acoustic and seismic energy during Strombolian eruptions. J. Volcanol. Geotherm. Res. 148, 334–354. https://doi.org/10.1016/j.jvolgeores.2005.05.002
Johnson, J.B., Ripepe, M., 2011. Volcano infrasound: A review. J. Volcanol. Geotherm. Res. 206, 61–69. https://doi.org/10.1016/J.JVOLGEORES.2011.06.006
Kantzas, E.P., McGonigle, A.J.S., Tamburello, G., Aiuppa, A., Bryant, R.G., 2010. Protocols for UV camera volcanic SO2 measurements. J. Volcanol. Geotherm. Res. 194, 55–60. https://doi.org/10.1016/j.jvolgeores.2010.05.003
Kern, C., Lübcke, P., Bobrowski, N., Campion, R., Mori, T., Smekens, J.-F., Stebel, K., Tamburello, G., Burton, M., Platt, U., Prata, F., 2015. Intercomparison of SO2 camera systems for imaging volcanic gas plumes. J. Volcanol. Geotherm. Res. 300, 22–36. https://doi.org/10.1016/j.jvolgeores.2014.08.026
Kern, C., Sutton, J., Elias, T., Lee, L., Kamibayashi, K., Antolik, L., Werner, C., 2014. An automated SO2 camera system for continuous, real-time monitoring of gas emissions from Kīlauea Volcano's summit Overlook Crater. J. Volcanol. Geotherm. Res. 300, 81–94. https://doi.org/10.1016/j.jvolgeores.2014.12.004
Kern, C., Werner, C., Elias, T., Sutton, A.J., Lübcke, P., 2013. Applying UV cameras for

SO2 detection to distant or optically thick volcanic plumes. J. Volcanol. Geotherm. Res. 262, 80–89. https://doi.org/10.1016/j.jvolgeores.2013.06.009

Klein, A., Lübcke, P., Bobrowski, N., Kuhn, J., Platt, U., 2017. Plume propagation direction determination with SO 2 cameras. Atmos. Meas. Tech 10, 979–987. https://doi.org/10.5194/amt-10-979-2017

Kremers, S., Wassermann, J., Meier, K., Pelties, C., van Driel, M., Vasseur, J., Hort, M., 2013. Inverting the source mechanism of Strombolian explosions at Mt. Yasur, Vanuatu, using a multi-parameter dataset. J. Volcanol. Geotherm. Res. 262, 104–122. https://doi.org/10.1016/j.jvolgeores.2013.06.007

Laiolo, M., Massimetti, F., Cigolini, C., Ripepe, M., Coppola, D., 2018. Long-term eruptive trends from space-based thermal and SO2 emissions: a comparative analysis of Stromboli, Batu Tara and Tinakula volcanoes. Bull. Volcanol. 80, 1–19. https://doi.org/10.1007/s00445-018-1242-0

Liu, E.J., Wood, K., Mason, E., Edmonds, M., Aiuppa, A., Giudice, G., Bitetto, M., Francofonte, V., Burrow, S., Richardson, T., Watson, M., Pering, T.D., Wilkes, T.C., McGonigle, A.J.S., Velasquez, G., Melgarejo, C., Bucarey, C., 2019. Dynamics of Outgassing and Plume Transport Revealed by Proximal Unmanned Aerial System (UAS) Measurements at Volcán Villarrica, Chile. Geochemistry, Geophys. Geosystems 20, 730–750. https://doi.org/10.1029/2018GC007692

Lübcke, P., Bobrowski, N., Illing, S., Kern, C., Alvarez Nieves, J.M., Vogel, L., Zielcke, J., Delgado Granados, H., Platt, U., 2013. On the absolute calibration of SO_2 cameras. Atmos. Meas. Tech. 6, 677–696. https://doi.org/10.5194/amt-6-677-2013

Marchetti, E., Ripepe, M., Harris, A.J.L., Delle Donne, D., 2009. Tracing the differences between Vulcanian and Strombolian explosions using infrasonic and thermal radiation energy. Earth Planet. Sci. Lett. 279, 273–281. https://doi.org/10.1016/j.epsl.2009.01.004

McGonigle, A.J.S., Aiuppa, A., Ripepe, M., Kantzas, E.P., Tamburello, G., 2009. Spectroscopic capture of 1 Hz volcanic SO2 fluxes and integration with volcano geophysical data. Geophys. Res. Lett. 36, 1–5. https://doi.org/10.1029/2009GL040494

McGonigle, A.J.S., Hilton, D.R., Fischer, T.P., Oppenheimer, C., 2005. Plume velocity determination for volcanic SO2 flux measurements. Geophys. Res. Lett. 32, 1–4. https://doi.org/10.1029/2005GL022470

McGonigle, A.J.S., Pering, T.D., Wilkes, T.C., Tamburello, G., D'Aleo, R., Bitetto, M., Aiuppa, A., Willmott, J.R., 2017. Ultraviolet Imaging of Volcanic Plumes: A New Paradigm in Volcanology. Geosciences 7, 68. https://doi.org/10.3390/geosciences7030068

Meier, K., Hort, M., Wassermann, J., Garaebiti, E., 2016. Strombolian surface activity regimes at Yasur volcano, Vanuatu, as observed by Doppler radar, infrared camera and infrasound. J. Volcanol. Geotherm. Res. 322, 184–195. https://doi.org/10.1016/j.jvolgeores.2015.07.038

Métrich, N., Allard, P., Aiuppa, A., Bani, P., Bertagnini, A., Shinohara, H., Parello, F., Di Muro, A., Garaebiti, E., Belhadj, O., Massare, D., 2011. Magma and Volatile Supply to Post-collapse Volcanism and Block Resurgence in Siwi Caldera (Tanna Island, Vanuatu Arc). J. Petrol. 52, 1077–1105. https://doi.org/10.1093/petrology/egr019

Mori, T., Burton, M., 2009. Quantification of the gas mass emitted during single explosions on Stromboli with the SO2 imaging camera. J. Volcanol. Geotherm. Res. 188, 395–400. https://doi.org/10.1016/j.jvolgeores.2009.10.005

Mori, T., Burton, M., 2006. The SO_2 camera: A simple, fast and cheap method for ground-based imaging of SO_2 in volcanic plumes. Geophys. Res. Lett. 33, L24804. https://doi.org/10.1029/2006GL027916

Oppenheimer, C., Bani, P., Calkins, J.A., Burton, M.R., Sawyer, G.M., 2006. Rapid FTIR sensing of volcanic gases released by Strombolian explosions at Yasur volcano, Vanuatu. Appl. Phys. B 85, 453–460. https://doi.org/10.1007/s00340-006-2353-4

Oppenheimer, C., Lomakina, A.S., Kyle, P.R., Kingsbury, N.G., Boichu, M., 2009. Pulsatory magma supply to a phonolite lava lake. Earth Planet. Sci. Lett. 284, 392–398. https://doi.org/10.1016/j.epsl.2009.04.043

Parfitt, E.A., 2004. A discussion of the mechanisms of explosive basaltic eruptions. J. Volcanol. Geotherm. Res. 134, 77–107. https://doi.org/10.1016/j.jvolgeores.2004.01.002

Patrick, M.R., Harris, A.J.L., Ripepe, M., Dehn, J., Rothery, D.A., Calvari, S., 2007. Strombolian explosive styles and source conditions: Insights from thermal (FLIR) video. Bull. Volcanol. 69, 769–784. https://doi.org/10.1007/s00445-006-0107-0

Pering, T.D., Ilanko, T., Liu, E.J., 2019a. Periodicity in Volcanic Gas Plumes: A Review and Analysis. Geosci. 2019, Vol. 9, Page 394 9, 394. https://doi.org/10.3390/GEOSCIENCES9090394

Pering, T.D., Ilanko, T., Wilkes, T.C., England, R.A., Silcock, S.R., Stanger, L.R., Willmott, J.R., Bryant, R.G., McGonigle, A.J.S., 2019b. A Rapidly Convecting Lava Lake at Masaya Volcano, Nicaragua. Front. Earth Sci. 6, 241. https://doi.org/10.3389/feart.2018.00241

Pering, T.D., Liu, E.J., Wood, K., Wilkes, T.C., Aiuppa, A., Tamburello, G., Bitetto, M., Richardson, T., McGonigle, A.J.S., 2020. Combined ground and aerial measurements resolve vent-specific gas fluxes from a multi-vent volcano. Nat. Commun. 11, 3039. https://doi.org/10.1038/s41467-020-16862-w

Pering, T.D., McGonigle, A.J.S., 2018. Combining Spherical-Cap and Taylor Bubble Fluid Dynamics with Plume Measurements to Characterize Basaltic Degassing. Geosciences 8, 42. https://doi.org/10.3390/geosciences8020042

Pering, T.D., McGonigle, A.J.S., James, M.R., Capponi, A., Lane, S.J., Tamburello, G., Aiuppa, A., 2017. The dynamics of slug trains in volcanic conduits: Evidence for expansion driven slug coalescence. J. Volcanol. Geotherm. Res. 348, 26–35. https://doi.org/10.1016/J.JVOLGEORES.2017.10.009

Pering, T.D., McGonigle, A.J.S., James, M.R., Tamburello, G., Aiuppa, A., Delle Donne, D., Ripepe, M., 2016. Conduit dynamics and post-explosion degassing on Stromboli: a combined UV camera and numerical modelling treatment. Geophys. Res. Lett. https://doi.org/10.1002/2016GL069001

Pering, T. D., McGonigle, A.J.S., James, M.R., Tamburello, G., Aiuppa, A., Delle Donne, D., Ripepe, M., 2016. Conduit dynamics and post explosion degassing on Stromboli: A combined UV camera and numerical modeling treatment. Geophys. Res. Lett. 43, 5009–5016. https://doi.org/10.1002/2016GL069001

Pering, T.D., Tamburello, G., McGonigle, A.J.S., Aiuppa, A., Cannata, A., Giudice, G., Patanè, D., 2014. High time resolution fluctuations in volcanic carbon dioxide degassing from Mount Etna. J. Volcanol. Geotherm. Res. 270, 115–121. https://doi.org/10.1016/j.jvolgeores.2013.11.014

Pering, T.D., Tamburello, G., McGonigle, A.J.S., Aiuppa, A., James, M.R., Lane, S.J., Sciotto, M., Cannata, A., Patanè, D., 2015. Dynamics of mild strombolian activity on Mt. Etna. J. Volcanol. Geotherm. Res. 300, 103–111. https://doi.org/10.1016/j.jvolgeores.2014.12.013

Peters, N., Hoffmann, A., Barnie, T., Herzog, M., Oppenheimer, C., 2015. Use of motion estimation algorithms for improved flux measurements using SO2 cameras. J. Volcanol. Geotherm. Res. 300, 58–69. https://doi.org/10.1016/j.jvolgeores.2014.08.031

Peters, N., Oppenheimer, C., 2018. Plumetrack: Flux calculation software for UV cameras. Comput. Geosci. 118, 86–90. https://doi.org/10.1016/j.cageo.2018.05.014

Platt, U., Lübcke, P., Kuhn, J., Bobrowski, N., Prata, F., Burton, M., Kern, C., 2015.

Quantitative imaging of volcanic plumes — Results, needs, and future trends. J. Volcanol. Geotherm. Res. 300, 7–21. https://doi.org/10.1016/j.jvolgeores.2014.10.006

Polacci, M., Baker, D.R.D., La Rue, Alexandra, Mancini, L., Allard, P., Rue, A La, Mancini, L., 2012. Degassing behaviour of vesiculated basaltic magmas: an example from Ambrym volcano, Vanuatu Arc 233–234, 55–64. https://doi.org/10.1016/J.JVOLGEORES.2012.04.019

Ripepe, M., Harris, A.J.L., Carniel, R., 2002. Thermal, seismic and infrasonic evidences of variable degassing rates at Stromboli volcano. J. Volcanol. Geotherm. Res. 118, 285–297. https://doi.org/10.1016/S0377-0273(02)00298-6

Ripepe, M., Harris, A.J.L., Marchetti, E., 2005. Coupled thermal oscillations in explosive activity at different craters of Stromboli volcano. Geophys. Res. Lett. 32, 1–4. https://doi.org/10.1029/2005GL022711

Ripepe, M., Marchetti, E., 2002. Array tracking of infrasonic sources at Stromboli volcano. Geophys. Res. Lett. 29, 33-1-33–4. https://doi.org/10.1029/2002gl015452

Salvatore, V., Cigala, V., Taddeucci, J., Arciniega-Ceballos, A., Peña Fernández, J.J., Alatorre-Ibargüengoitia, M.A., Gaudin, D., Palladino, D.M., Kueppers, U., Scarlato, P., 2020. Gas-Pyroclast Motions in Volcanic Conduits During Strombolian Eruptions, in Light of Shock Tube Experiments. J. Geophys. Res. Solid Earth 125. https://doi.org/10.1029/2019JB019182

Salvatore, V., Silleni, A., Corneli, D., Taddeucci, J., Palladino, D.M., Sottili, G., Bernini, D., Andronico, D., Cristaldi, A., 2018. Parameterizing multi-vent activity at Stromboli Volcano (Aeolian Islands, Italy). Bull. Volcanol. 80, 64. https://doi.org/10.1007/s00445-018-1239-8

Seyfried, R., Freundt, A., 2000. Experiments on conduit flow and eruption behavior of basaltic volcanic eruptions. J. Geophys. Res. 105, 23727. https://doi.org/10.1029/2000JB900096

Shinohara, H., Ohminato, T., Takeo, M., Tsuji, H., 2015. Monitoring of volcanic gas composition at Asama volcano, Japan, during 2004–2014. J. Volcanol.

Shinohara, H., Witter, J.B., 2005. Volcanic gases emitted during mild Strombolian activity of Villarrica volcano, Chile. Geophys. Res. Lett. 32, L20308. https://doi.org/10.1029/2005GL024131

Simons, B.C., Jolly, A.D., Eccles, J.D., Cronin, S.J., 2020. Spatiotemporal Relationships between Two Closely-spaced Strombolian-style Vents, Yasur, Vanuatu. Geophys. Res. Lett. 47. https://doi.org/10.1029/2019GL085687

Spina, L., Taddeucci, J., Cannata, A., Gresta, S., Lodato, L., Privitera, E., Scarlato, P., Gaeta, M., Gaudin, D., Palladino, D.M., 2016. “Explosive volcanic activity at Mt. Yasur: A characterization of the acoustic events (9–12th July 2011).” J. Volcanol. Geotherm. Res. 322, 175–183. https://doi.org/10.1016/j.jvolgeores.2015.07.027

Spina, A. La, Burton, M.R., Harig, R., Mure, F., Rusch, P., Jordan, M., Caltabiano, T., 2013. New insights into volcanic processes at Stromboli from Cerberus , a remote-controlled open-path FTIR scanner system. J. Volcanol. Geotherm. Res. 249, 66–76. https://doi.org/10.1016/j.jvolgeores.2012.09.004

Suckale, J., Keller, T., Cashman, K. V., Persson, P.O., 2016. Flow-to-fracture transition in a volcanic mush plug may govern normal eruptions at Stromboli. Geophys. Res. Lett. 43, 12,071-12,081. https://doi.org/10.1002/2016GL071501

Suckale, J, Keller, T., Cashman, K. V, Persson, P.-O., 2016. Flow-to-fracture transition in a volcanic mush plug may govern normal eruptions at Stromboli. Geophys. Res. Lett. 43, 12071–12081. https://doi.org/10.1002/2016GL071501

Sweeney, D., Kyle, P.R., Oppenheimer, C., 2008. Sulfur dioxide emissions and degassing behavior of Erebus volcano, Antarctica. J. Volcanol. Geotherm. Res. 177, 725–733.

https://doi.org/10.1016/j.jvolgeores.2008.01.024
Szramek, L., Gardner, J.E., Larsen, J., 2006. Degassing and microlite crystallization of basaltic andesite magma erupting at Arenal Volcano, Costa Rica. J. Volcanol. Geotherm. Res. 157, 182–201. https://doi.org/10.1016/j.jvolgeores.2006.03.039
Taddeucci, J., Edmonds, M., Houghton, B., James, M.R., Vergniolle, S., 2015. Hawaiian and Strombolian Eruptions, in: The Encyclopedia of Volcanoes. Elsevier, pp. 485–503. https://doi.org/10.1016/b978-0-12-385938-9.00027-4
Taddeucci, J., Scarlato, P., Capponi, A., Del Bello, E., Cimarelli, C., Palladino, D.M., Kueppers, U., Bello, E. Del, Cimarelli, C., Palladino, D.M., Kueppers, U., 2012. High-speed imaging of Strombolian explosions: The ejection velocity of pyroclasts. Geophys. Res. Lett. 39, 1–6. https://doi.org/10.1029/2011GL050404
Tamburello, G., Aiuppa, A., Kantzas, E.P., Mcgonigle, A.J.. S., Ripepe, M., 2012. Passive vs . active degassing modes at an open-vent volcano (Stromboli , Italy). Earth Planet. Sci. Lett. 359–360, 106–116. https://doi.org/10.1016/j.epsl.2012.09.050
Tamburello, G., Aiuppa, A., McGonigle, A.J.S., Allard, P., Cannata, A., Giudice, G., Kantzas, E.P., Pering, T.D., 2013. Periodic volcanic degassing behavior: The Mount Etna example. Geophys. Res. Lett. 40, 4818–4822. https://doi.org/10.1002/grl.50924
Thielicke, W., 2014. The flapping flight of birds : analysis and application. [S.n.].
Thielicke, W., Stamhuis, E.J., 2014. PIVlab – Towards User-friendly, Affordable and Accurate Digital Particle Image Velocimetry in MATLAB. J. Open Res. Softw. 2. https://doi.org/10.5334/jors.bl
Vergniolle, S., Boichu, M., Caplan-Auerbach, J., 2004. Acoustic measurements of the 1999 basaltic eruption of Shishaldin volcano, Alaska 1. Origin of Strombolian activity. J. Volcanol. Geotherm. Res. 137, 109–134. https://doi.org/10.1016/j.jvolgeores.2004.05.003
Vergniolle, S., Jaupart, C., 1986. Separated two-phase flow and basaltic eruptions. J. Geophys. Res. Solid Earth 91, 12842–12860. https://doi.org/10.1029/JB091iB12p12842
Wilkes, T., McGonigle, A., Pering, T., Taggart, A., White, B., Bryant, R., Willmott, J., Wilkes, T.C., McGonigle, A.J.S., Pering, T.D., Taggart, A.J., White, B.S., Bryant, R.G., Willmott, J.R., 2016. Ultraviolet Imaging with Low Cost Smartphone Sensors: Development and Application of a Raspberry Pi-Based UV Camera. Sensors 16, 1649. https://doi.org/10.3390/s16101649
Wilkes, T., Pering, T., McGonigle, A., Tamburello, G., Willmott, J., Wilkes, T.C., Pering, T.D., McGonigle, A.J.S., Tamburello, G., Willmott, J.R., 2017. A Low-Cost Smartphone Sensor-Based UV Camera for Volcanic SO2 Emission Measurements. Remote Sens. 9, 27. https://doi.org/10.3390/rs9010027
Williams-Jones, G., Horton, K.A., Elias, T., Garbeil, H., Mouginis-Mark, P.J., Sutton, A.J., Harris, A.J.L., 2006. Accurately measuring volcanic plume velocity with multiple UV spectrometers. Bull. Volcanol. 68, 328–332. https://doi.org/10.1007/s00445-005-0013-x
Woitischek, J., Woods, A.W., Edmonds, M., Oppenheimer, C., Aiuppa, A., Pering, T.D., Ilanko, T., D'Aleo, R., Garaebiti, E., 2020. Strombolian eruptions and dynamics of magma degassing at Yasur Volcano (Vanuatu). J. Volcanol. Geotherm. Res.